Generalizing TiO_2 Atom-Centred Symmetry Function Neural Network Potentials to Other Titanium Oxides

Austin Zhu

PHYS 310, Winter Term 2 2024-2025

Instructor: Dr. Jörg Rottler

University of British Columbia

April, 2025

Abstract

Symmetry functions are motivated by literature and used to featurize a bulk TiO_2 dataset. Two different neural network potential models using different sets of symmetry functions (G^2 and G^4, and G^2 only) are optimized and compared, resulting in the discovery that radial symmetry functions are more relevant in this dataset than angular symmetry functions. Optimal models predict the potentials of assorted titanium oxide crystals but fail to validly predict trends, showing the poor generalizability of neural network potentials.

1 Introduction

The aim of this paper is to test the feasibility of extending an neural network potential trained on specific species to other similar species, in this case with the same constituent elements. The research question is then, "to what extent can symmetry function trained neural network potentials be extended to species with the same constituent elements?".

1.1 Motivation for Calculating Potential-Energy Surfaces (PESs)

The primary motivation for developing potential-energy surfaces is for accurate molecular dynamics and Monte-Carlo simulations [1]. Quite similar to classical mechanics, knowing the potential energy as a function of position means the dynamics of the system can be solved. A variety of methods exist to determine these PESs: Traditional wave-function methods such as Hartree-Fock plus Configuration Interaction or many-body perturbation theory determine the surface by solving for the wave-function of the system, allowing the retrieval of the PES. However, these are computationally intensive and require copious storage. Less intensive are DFT methods, calculating the PES for the narrowed, pertinent environment. Still, these methods end up being computationally intensive [2].

1.2 Behler–Parrinello artificial neural network (ANN) potentials

This project is based in large part on two groups of work: Behler and Parinello's work with eponymous Behler–Parrinello ANN potentials [3][4][5], and Artrith and Urban's work with **ænet** [6]. Artrith and Urban constructed **ænet**, a library for training and determining Behler-Parrinello ANN potentials, using a TiO_2 dataset as a benchmark – the same dataset is used in this paper.

These ANNs are a less computationally intensive way of calculating PSEs, but require more work optimizing and training in a way that can generalize for a given material [3].

1.3 Symmetry Functions

To use ANNs to generate potentials, featurization for the neural network input is paramount. To see why symmetry functions are used, consider first the naive approach of using atomic positions as features: within a sample, the positions of each atom is known. In this case, the atomic environment is certainly the same environment whether or not it has been rotated or translated, however, the features are *not* invariant under rotations or translations. Similarly, permuting elements, such as swapping the two hydrogens of a water molecule, should remain identical, but each of the hydrogens has a unique input and resulting weights in the neural network [5]. Feeding in only atomic coordinates is a possible method, and processes that generate spatially constrained higher order structures such as convolutional neural networks (CNN) may be used to produce potentials. Higher order structures, such as the distances

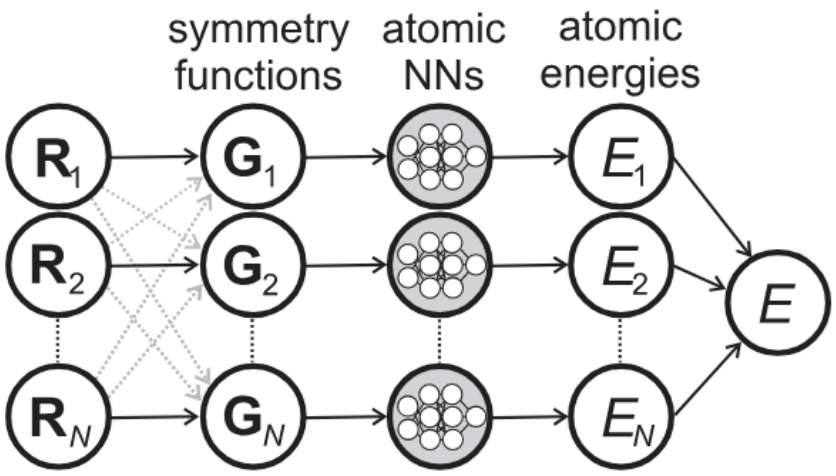

Figure 1: Behler and Parinello's forward-feed neural networks first employed in the 2007 paper [3]. The first layer (R_n^α) represent the positions of the nth indexed atom. These feed into the symmetry functions G_i^μ, which are processed through neural networks and summed into a final energy. Note in this paper, the central NN layers are a multi-layer perceptron (MLP) as utilized in Artrith and Urban's 2015 work [6]. Image retrieved from Behler and Parinello 2011 [4].

between atoms, are not directly provided to the neural network, so relatively little work needs to be done to achieve reasonable results [7].

However, Behler and Parinello's work seeks to input higher-dimensional structures, such as interatomic distance, directly into the neural network, developing a high-dimensional neural network potential. Symmetry functions are chosen that convert the atomic position input into values that avoid issues of variation from rotation, translation, or permutation, as well as removing some of the burden from the ANN to develop higher dimension structures [5].

So, Behler and Parinello choose symmetry functions by the criteria [5]:

1. "rotational and translational invariance"
2. "invariance with respect to the permutation of atoms of the same element
3. "provide a unique description of the atomic positions"
4. "constant number of function values independent of the number of atoms in the cutoff spheres"

Points 1 and 2 have already been discussed above. Furthermore, stated in point 3, the functions must be useful enough to meaningfully extract potentials – otherwise, a constant

function would suffice the previous two requirements. Finally, in point 4, there should not be a dependence on the number of atoms in the relevant environment, as this will change throughout a molecular dynamics calculation, and would require a changing neural network architecture.

A notable shortcoming of symmetry function featurization is the increasing computational load with increasing the size of the sample, as every atom is considered in the symmetry function [5]. This is avoided with the pertinent datasets in this paper as they are all fairly small and/or periodic.

The relevant symmetry functions are the G^2 and G^4 functions. As this paper uses the 2007 Behler and Parinello [3], and Artrith and Urban [6] papers as qualitative benchmarks, the same symmetry functions are used.

Symmetry functions are divided into two types: radial, and angular. Radial functions are two-body functions, concerned with one central atom (hence atom-centred) and summed over every other atom. Angular functions are concerned with one central atom and summed over every other pair or greater grouping of other atoms, being three-bodied or higher functions. The qualitative benchmark papers use one radial and one angular symmetry function in total, the G^2 and G^4 functions respectively.

1.4 G^2 Symmetry Function

The radial G^2 function (first called G^1 in Behler and Parinello, 2007[3]) is defined as

$$G_i^2 = \sum_{j \neq i}^{\text{all}} e^{-\eta(R_{ij}-R_s)^2} f_c(R_{ij}).$$

where η and R_s are tunable parameters [5]. f_c is a cutoff radius function, which defines a local and atom-centred region the symmetry function is concerned with. This is defined, first by Behler and Parinello [3], as

$$f_c(R_{ij}) = \begin{cases} 0.5 \times \left[\cos\left(\frac{\pi R_{ij}}{R_c}\right) + 1\right] & \text{for } R_{ij} \leq R_c, \\ 0 & \text{for } R_{ij} > R_c. \end{cases}$$

Note that atoms past a distance R_c will contribute nothing. With the definition of the cutoff function, the G^2 function can be described as a spherical shell around the central atom, with

thickness and location of the shell defined by the Gaussian parameters η and R_s respectively, as shown in Figure 2. In fact, matching the standard form of a Gaussian,

$$\eta = \frac{1}{2\sigma^2}$$
$$R_s = \mu$$

relates R_s and η to the mean and standard deviation parameters of the Gaussian.

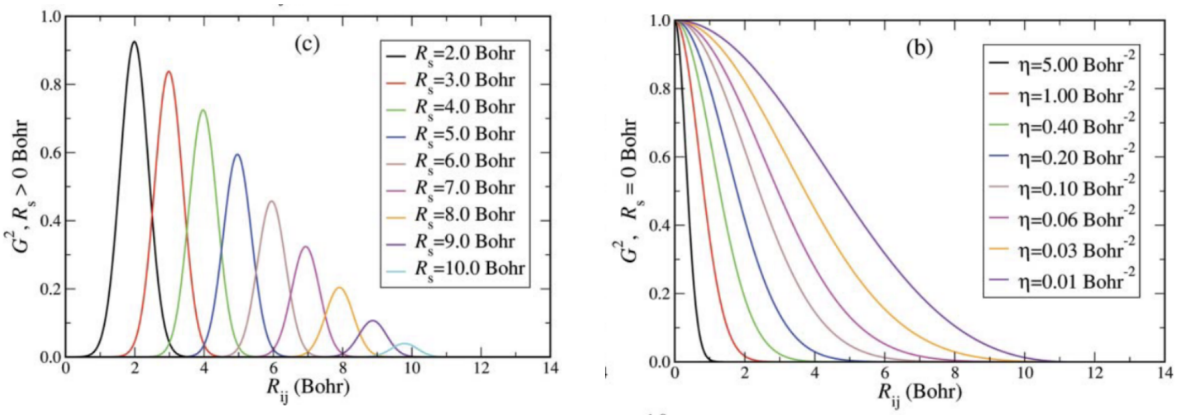

Figure 2: Effects of parameters η shell width, and R_s shell distance on the G^2 function. This aids the choice of pertinent values of each parameter. Image retrieved from Behler and Parinello, 2011 [4]

1.5 G^4 Symmetry Function

The angular symmetry function G^4 (originally G^2 in Behler and Parinello, 2007 [3]) is defined as

$$G_i^4 = 2^{1-\zeta} \sum_{j,k\neq i}^{\text{all}} (1 + \lambda \cos\theta_{ijk})^\zeta \cdot e^{-\eta(R_{ij}^2+R_{ik}^2+R_{jk}^2)} \cdot f_c(R_{ij}) \cdot f_c(R_{ik}) \cdot f_c(R_{jk}),$$

where ζ and λ are tunable parameters. Note the angle term in the cosine, which is defined as the angle made by the other two atoms j, k centred on atom i [5]. G^4 is therefore a three-body function. Once again, the cutoff function is applied such that triplets of atoms where any two are too far apart will not be considered.

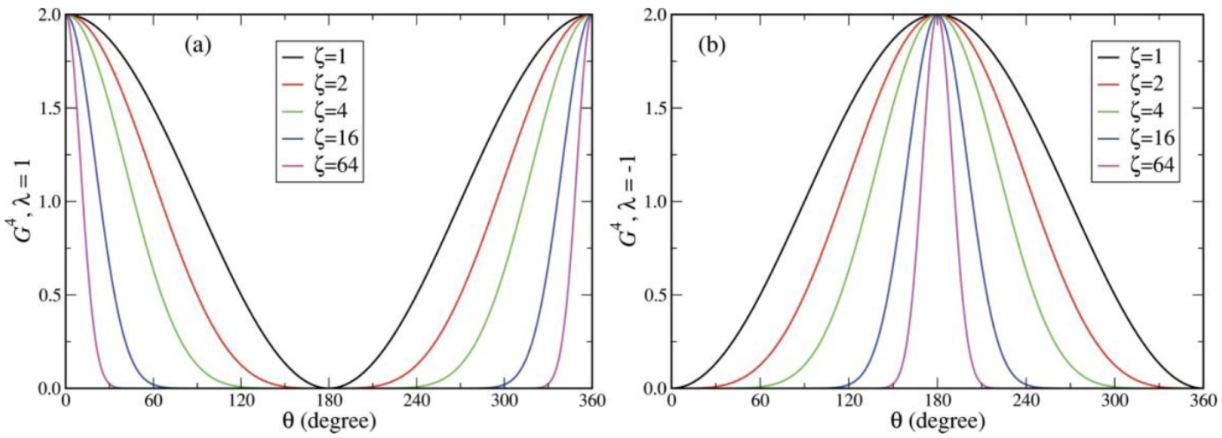

Figure 3: Effects of parameters ζ angular resolution, and λ, maximum of the cosine, on the G^4 function. This aids the choice of pertinent values of each parameter. Image retrieved from Behler and Parinello, 2011 [4]

The ζ parameter is an angular resolution, as shown in Figure 3, and λ determines whether the maximum of the cosine is at $\theta_{ijk} = 0$ or $\theta_{ijk} = \pi$, so takes the values $\lambda = -1, 1$.

2 Methods

The DScribe, scikit-learn, and TensorFlow libraries are used to featurize and train models. A cutoff radius of $R_c = 6$Å, as bond lengths of Ti-Ti are between 1–2Å[8], Ti-O bond lengths are approximately 2Å[9], and O-O bond lengths are 2.7Å[10]. So, the cutoff allows more than 2 bonds within the radius, as recommended and consistently used by Behler and Parinello[3][4].

The general workflow of this paper is to load the TiO_2 database provided in Artrith and Urban [6], linked on the **ænet** site here. Then, features in the form of symmetry function values are calculated. The features are scaled and used as inputs to a MLP, from where hyperparameter optimization is used through a random search to determine the best model. Cross-validation is used to determine the best score and resultant model. Lastly, the resultant model is applied to other titanium oxide structures sourced from The Materials Project, and those predicted energies are compared to DFT calculated energies also sourced from The Materials Project.

2.1 Featurization

The DScribe library, *dscribe.descriptors.acsf* module contains a class that can calculate symmetry function values provided an Atomic Simulation Environment (ASE) object.

There are *two* models trained in this paper: one using only the G^2 symmetry function, and one using both G^2 and G^4 symmetry functions. The motivation for having two models is to determine whether one works better for the purpose of determining energy/atom, and to determine an optimal set of symmetry functions that can generalize to other titanium oxides. No model is constructed without the radial G^2 function, as radial distance between two atoms is paramount to determining energy of a configuration by determining interatomic bonds [4].

Parameters are chosen to construct a feature set: R_s and σ (the standard deviation of the Gaussian in G^2) parameters are chosen to range evenly from 0 to R_c. η is then calculated from these σ values. ζ is chosen to range from high spread (1) to low spread (16) as shown in Figure 3. λ only takes values of $-1, 1$.

Parameter	**Range / Options**	**Notes**
R_c	6.0 Å	Cutoff radius for all symmetry functions
R_s (G^2)	0.00 – 6.00 Å	Step size = 0.55
σ (G^2, G^4)	0.5 – 6 Å	Step size = 0.5
η (G^2, G^4)	$1/(2\sigma^2)$	Cannot have $\sigma = 0$
ζ (G^4)	$1, 2, 4, 8, 16$	
λ (G^4)	$1, -1$	

Table 1: Parameters used for G^2 and G^4 symmetry functions. Note that σ does not include 0, as this would be a singularity in the Gaussian function. Each feature value is the result of one choice of values from each of the above parameters.

2.2 Model

A multi-layer perception (MLP) is used as the ANN of this paper. Feed-forward neural networks were utilized by Behler and Parinello, of which a MLP is one example. Artrith and Urban specifically use a MLP, so those results may be compared to those of the models developed in this paper.

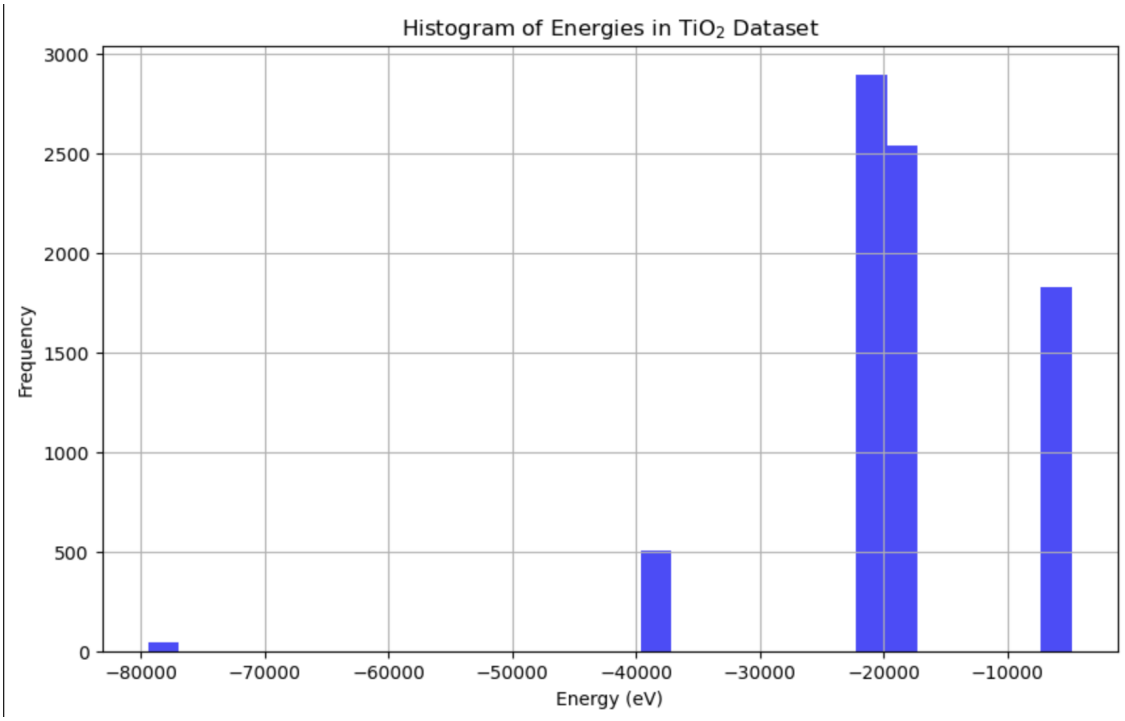

Figure 4: Histogram of energies of each sample set of atoms in the Artrith and Urban TiO_2. Note the cluster of samples at approximately -80000, -40000, -20000, and -5000 eV

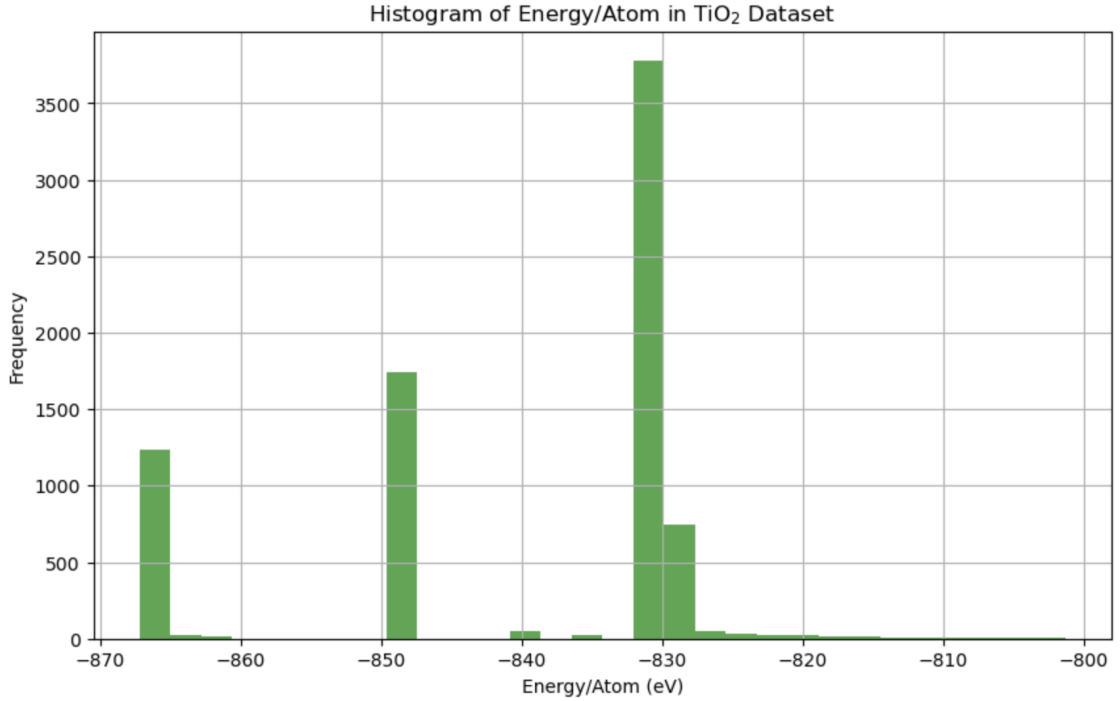

Figure 5: Histogram of energies per atom of each sample set of atoms in the Artrith and Urban TiO_2 dataset. Note the cluster of samples at approximately -865, -850, -830 eV

2.3 Targets

Notably, energy per atom is chosen as a target by Artrith and Urban [6], which is also used in this paper. This is due to the dataset having groupings of samples with total energy at four energy values due to each of these samples in a grouping having similar numbers of atoms (Figure 4). Energy per atom is visualized in 5, where there are still distinct groupings of samples at approximately -865, -850, -830 eV. However, these groupings can be attributed to the three possible natural polymorphs of TiO_2 represented in the dataset, rutile (the most common phase), anatase, and brookite [6]. The groupings of energy/atom samples is not a problem, as the number of atoms is should not affect the target but the structure of the sample certainly should.

2.4 Hyperparameter Optimization

The TensorFlow Keras library is used for hyperparameter optimization. A tuner is provided a broad grid of MLP hyperparameters to search. Then, a second search is conducted restricting to the optimal optimizer and a narrowed numeric range as determined by the retrieved best parameters by the first search. For both searches, a random search is used, by selecting a set of values or choices within the hyperparameter space and training with those.

2.5 Generalizing to Other Titanium Oxides

Titanium oxide crystal structures are retrieved from The Materials Project by their built-in API. These structures are then featurized with the same parameters as the TiO_2 where trained on. Saved models and scalers are applied to these structures, and the results can be examined to see how well the models have generalized to other titanium oxides.

3 Results

3.1 G^2 and G^4 model

In the first hyperparameter optimization for the Sequential G^2 and G^4 model, the following parameters are optimized: size of input layer, number of hidden layers, units in each hidden layer, dropout rate, and optimizers (Adam, RMSprop, or Adamax). The search is given 50

maximum trials of 5 executions with 50 epochs each, which narrows down the scope of the optimal hyperparameters.

Hyperparameter	**Type**	**Range / Options**	**Notes**
`units_input`	Integer	64 – 512	Step size = 64
`num_layers`	Integer	1 – 3	Number of hidden layers
`units_i`	Integer	32 – 512	Step size = 32
`dropout`	Float	0.0 – 0.5	Step size = 0.05
`optimizer`	Categorical	`adam`, `rmsprop`, `adamax`	

Table 2: First hyperparameter search space for the G^2 and G^4 model, and G_2 only model.

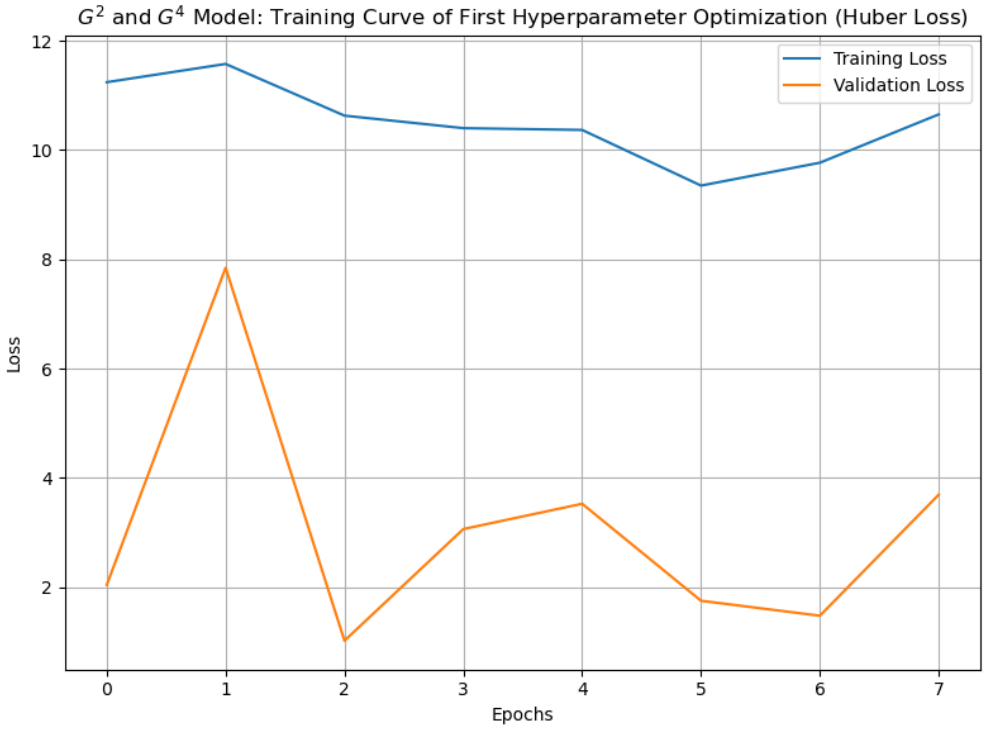

Figure 6: First hyperparameter optimization optimal G^2 and G^4 model training curve. There is visible under-fitting, as seen from the gap between training and validation loss.

Reflecting on the learning curve of this first search (Figure 6), the model is underfit – there is a visible gap between the training and validation losses. A second hyperparameter search is performed, searching through a narrower range of layer and unit amounts. The reduced search only uses the discovered best optimizer, Adamax, but adds a search through activation functions `relu` and `elu`. 30 maximum trials of 5 executions with 40 epochs each are used, representing a reduced random search.

Hyperparameter	Type	Range / Options	Notes
`units_input`	Integer	64 – 384	Step size = 64
`num_layers`	Integer	2 – 3	
`units_i`	Integer	128 – 768	Step size = 128
`dropout`	Float	0.1 – 0.3	Step size = 0.05
`activation`	Categorical	`relu`, `elu`	Previously only `elu`
`learning_rate`	Float (log)	10^{-4} – 10^{-2}	Log-uniform sampling
`optimizer`	Categorical	`adamax`	Chosen based on first search

Table 3: Second hyperparameter search space for the G^2 and G^4 model.

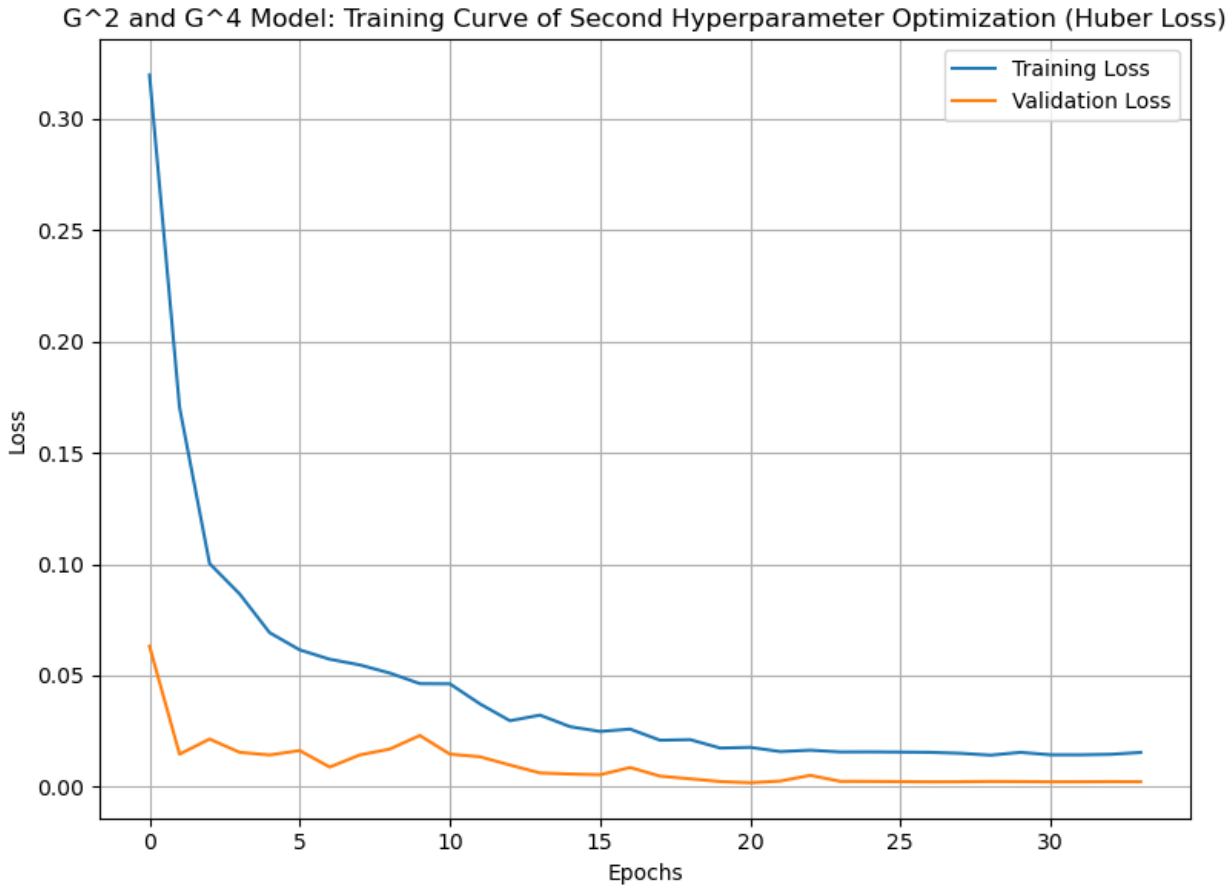

Figure 7: Second hyperparameter optimization optimal G^2 and G^4 model training curve. This is in an optimal regime, as there is a very small gap between the plateauing training and validation losses.

The result of the second hyperparameter search is a well optimized model, with a minimal gap between the plateauing training and validation losses (Figure 7). We may also compare the predicted vs ground truth graphs for each, which show outliers for both results. However, the deviation of outliers of the first hyperparameter search are significantly larger

in magnitude and show a trend towards the higher energy values that is not accounted for by the model 8. A trend exists for both results, but is less prominent after the second hyperparameter search.

3.2 G^2 only model

The first hyperparameter optimization is the same between the G^2 only model, and the G^2 and G^4 model. So, the parameters are the same as from Table 2

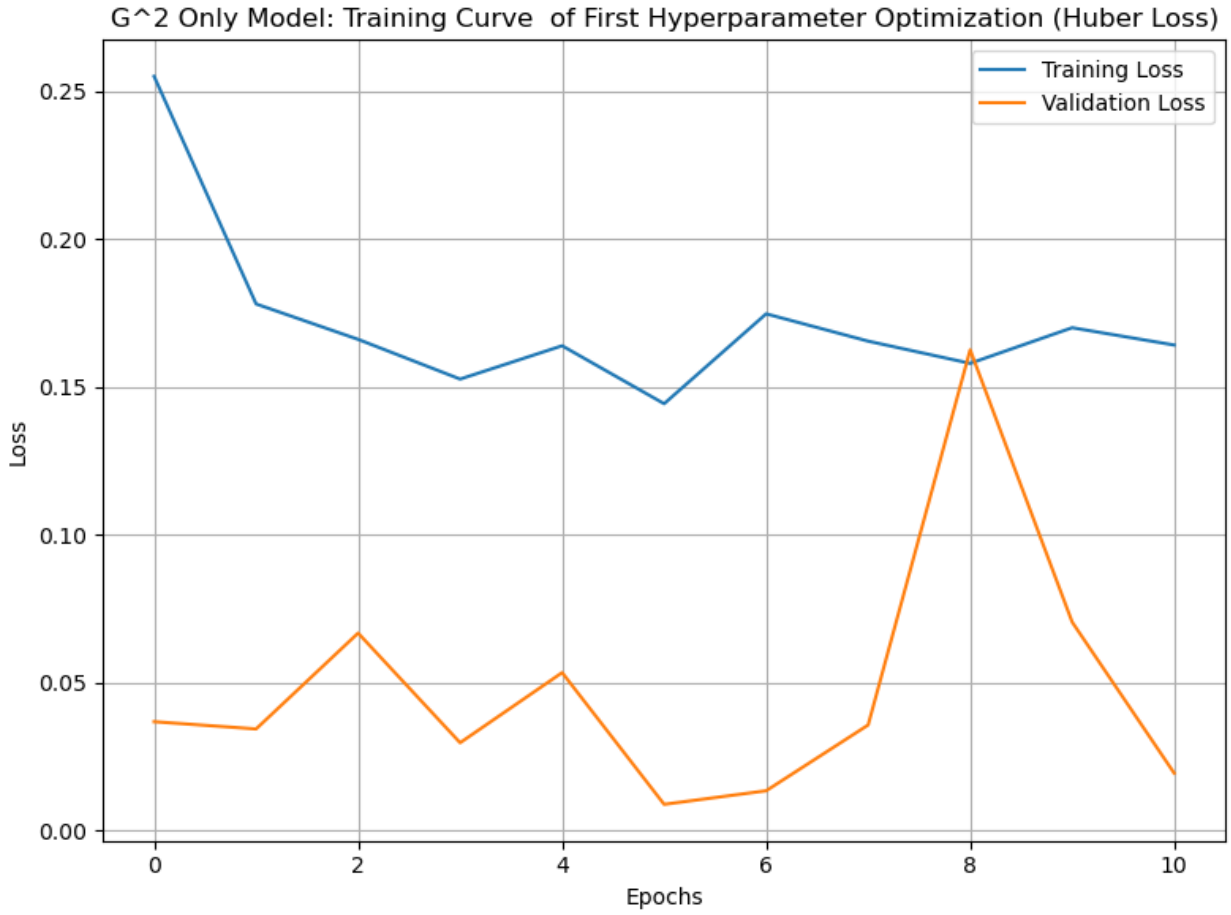

Figure 9: First hyperparameter optimization optimal G^2 only model training curve. There is visible under-fitting, as seen from the gap between training and validation loss.

The second hyperparameter search (Table 4) for the G^2 only model further searches through batch sizes, activation functions, dropout rate, learning rate, and number of layers. Once again, a narrower range of layer and unit amounts is used, and only the best optimizer, `Adamax`, is used. Additionally, final dropout is an option for the search, as well as batch

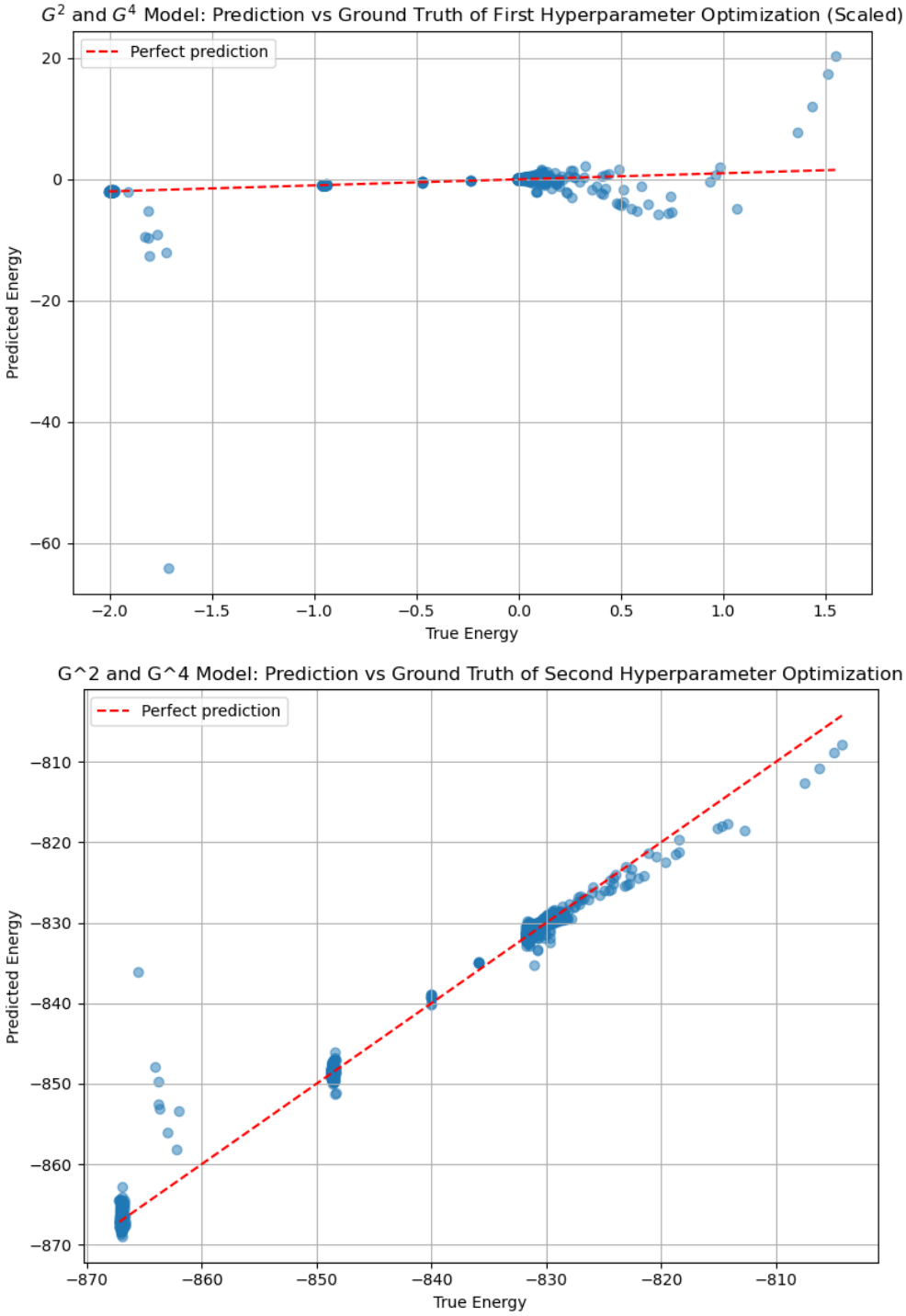

Figure 8: Prediction vs ground truth of first (above) and second (below) hyperparameter optimizations for G^2 and G^4 model. Note the more prevalent and further outliers in the result of the first hyperparameter optimization. Further note that the axes of the above are scaled.

normalization (with the inclusion of batch size options). The search is performed through 30 maximum trials of 5 executions with 40 epochs each, a reduced random search.

Hyperparameter	**Type**	**Range / Options**	**Notes**
`units_input`	Integer	64 – 384	Step size = 64
`num_layers`	Integer	1 – 3	
`units_i`	Integer	128 – 768	Step size = 128
`dropout`	Float	0.1 – 0.4	Step size = 0.05
`final_dropout`	Boolean	True, False	Optional final dropout layer
`final_dropout_rate`	Float	0.05 – 0.3	Step size = 0.05
`activation`	Categorical	`relu`, `elu`	Activation function for all layers
`learning_rate`	Float	10^{-4} – 10^{-2}	Log scale sampling
`use_batch_norm`	Boolean	True, False	Use batch normalization
`batch_size`	Integer	16 – 128	Step size = 16

Table 4: Second hyperparameter search space for the G^2 only model.

The final model is then saved, with result scores printed, predicted vs ground truth graphs, and residual graphs to visually determine if the model is correct.

3.3 Comparing Model Performances to Literature Results

The numerical benchmark set by Artrith and Urban is 5 meV/atom, and in that paper a minimum below 5 meV/atom is reached. The root mean squared error (RMSE) of 2.5 meV/atom is reached, and a mean absolute error (MAE) of 1 meV/atom is reached [6].

The optimal G^2 and G^4 model reaches RMSE of 1.273 eV/atom and MAE or 0.572 eV/atom. This is several orders of magnitude above the desired benchmark, and even further from the results reached by Artrith and Urban. This means this model does result in as good of a model as literature results.

However, the optimal G^2 model reaches RMSE of 62.2 meV/atom and MAE of 38.3 meV/atom. This is significantly lower than the optimal G^2 and G^4 model, showing that the G^2 only model is better. Although this is still an order of magnitude worse than the literature model, it is still remarkably good and can be considered a successful model. In comparing the magnitude of error to the energy/atom of the samples, notably the samples

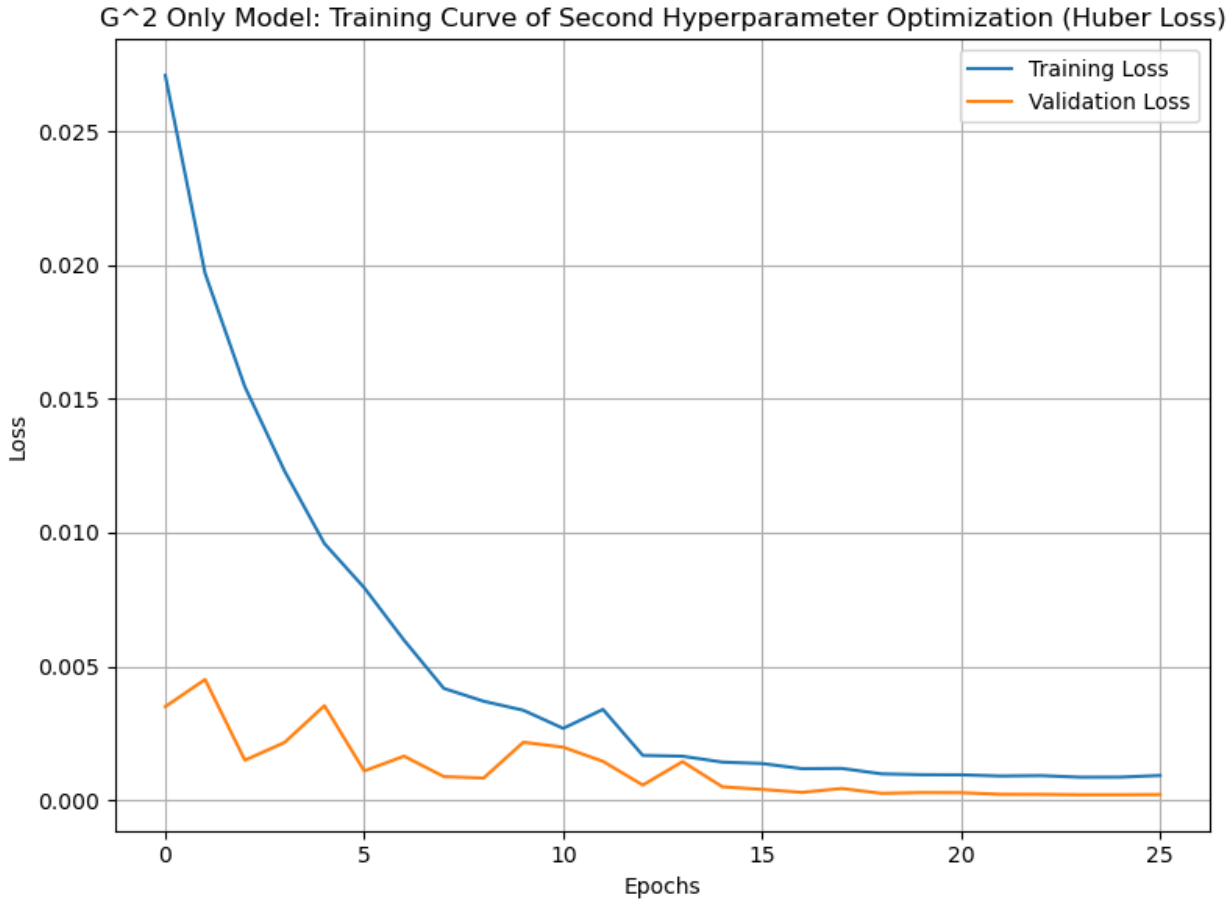

Figure 10: Second hyperparameter optimization optimal G^2 only model training curve. This is in an optimal regime, as there is a very small gap between the plateauing training and validation losses.

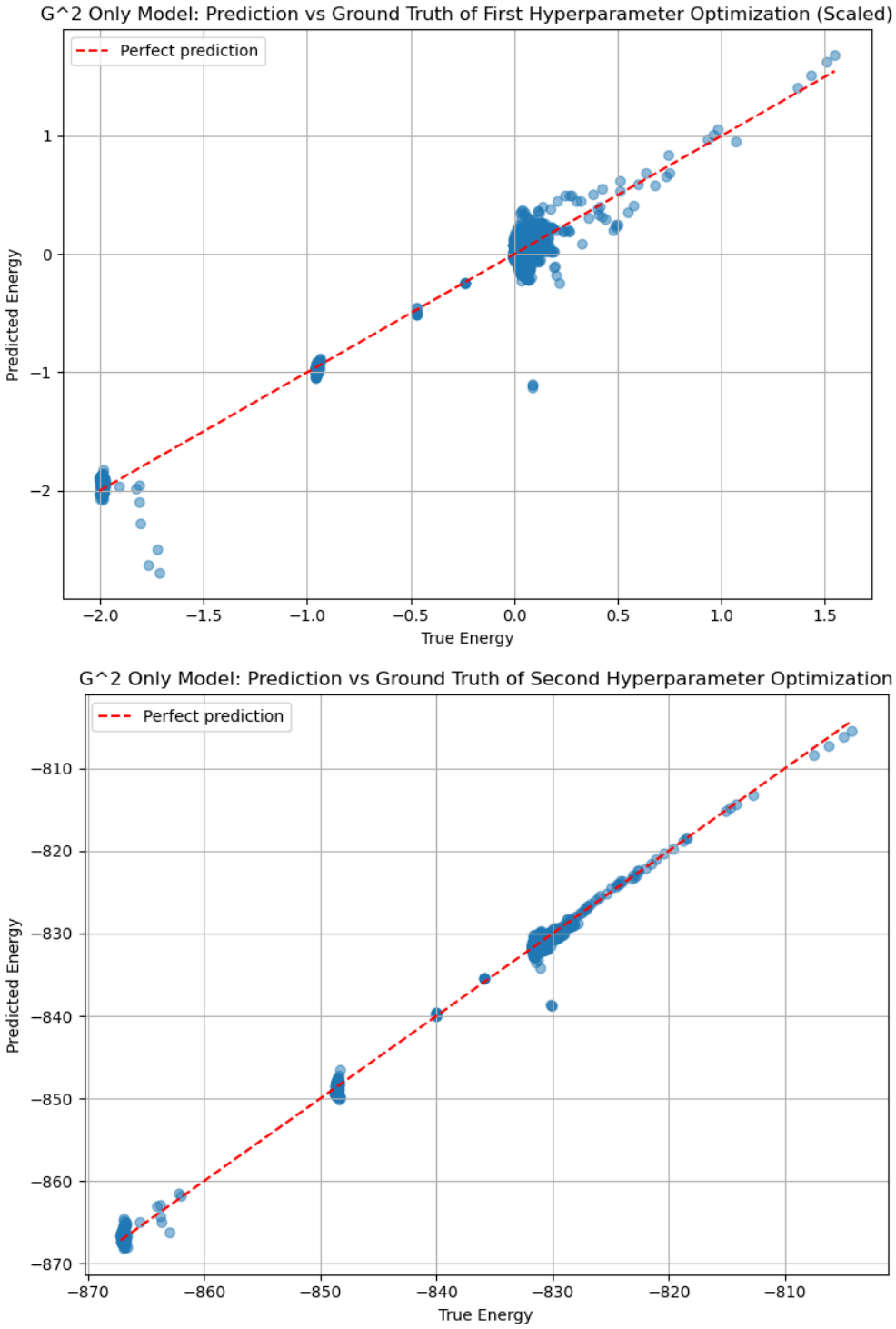

Figure 11: Prediction vs ground truth of first (above) and second (below) hyperparameter optimizations for G^2 only model. Note the more prevalent and further outliers in the result of the first hyperparameter optimization. Further note that the axes of the above are scaled.

have energies of 800 eV/atom, which is several orders of magnitude above both the RMSE and MAE.

In consideration of Artrith and Urban's results, the G^2 only model is comparable, and the G^2 and G^4 model is worse.

3.4 Comparing G^2 and G^4 model, and G^2 only model

As seen in Figure 8 and 11, there is a visible trend in the greater energy values for the G^2 and G^4 model. This trend is missing from the G^2 only model, showing that the G^2 only performs better. Examining the residual graphs, the trend is apparent and the magnitudes of deviation from perfect predictions are greater for the G^2 and G^4 model. Also considering the above discussion on error scores, it is evident that the G^2 only model performs measurably better.

This may in part be due to the higher relevance of interatomic distances (G^2) compared to angular features (G^4) for calculating energy, which may instead present G^4 values as noise instead of useful features. In that case, the model struggles to properly handle the increased noise and only performs better when given the relevant features.

3.5 Results of Generalizing to Other Titanium Oxides

Other titanium oxides are retrieved and processed, and an initial graph of predicted vs ground truth energies shows that there is some amount of offset energy, as the points are far below the perfect prediction line in Figure 13.

The energy offset is theorized to be the result of comparing bulk structures in the TiO_2 dataset, compared to single crystals in the retrieved titanium oxides. This is attempted to be removed by averaging the energy offset and removing the offset from every prediction value, leading to improved but still poor results.

Note that there is some trend successfully noted in the higher energy values, but the majority of samples around -9 eV/atom are unable to be matched correctly. The loss scores are fairly similar between the two models, as shown in Table 5.

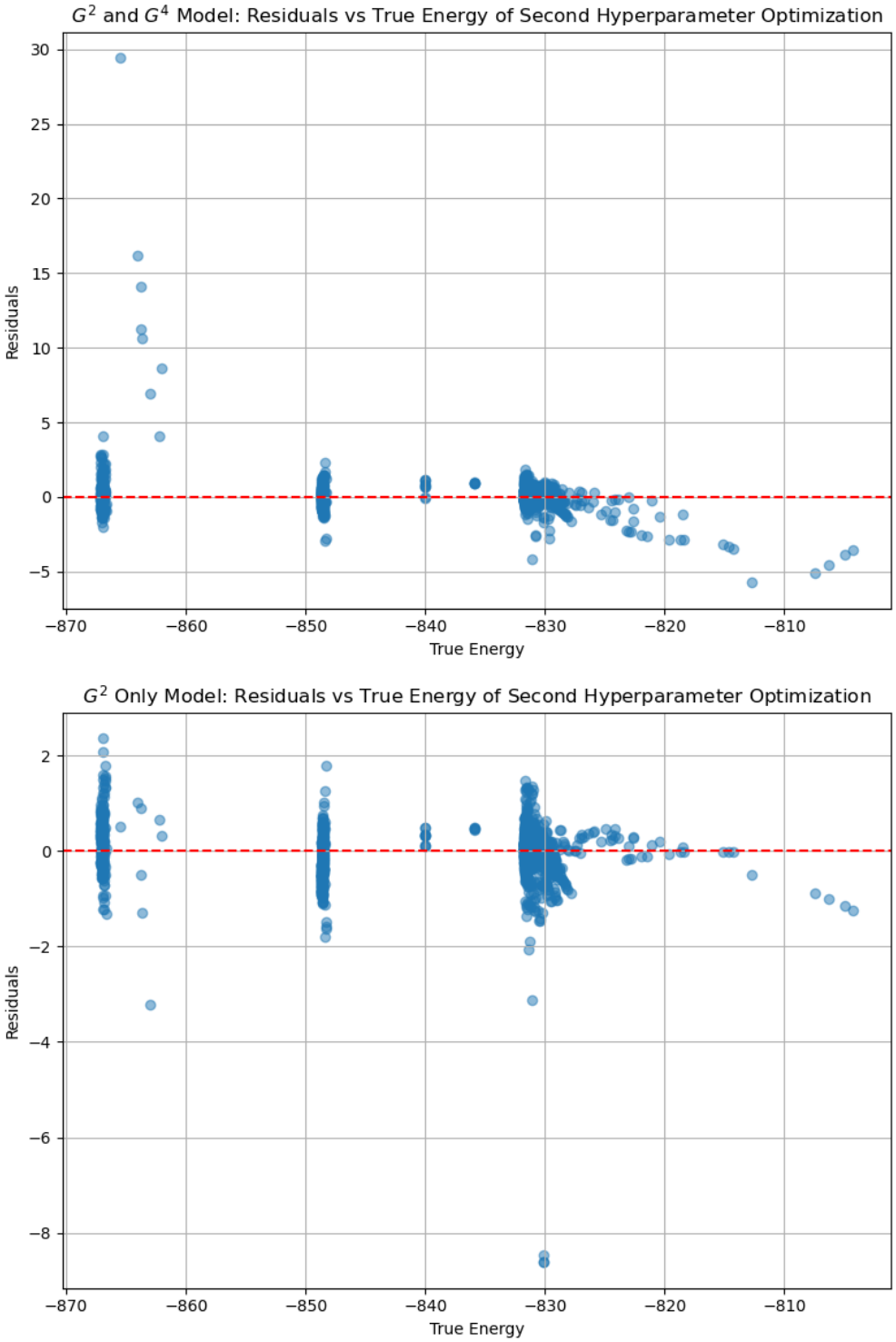

Figure 12: Residuals for optimal models found for G^2 and G^4 model (above), and G^2 only model (below). Note the reduced magnitude of residuals in the G^2 only model and the lack of trend on the right side, compared to the G^2 and G^4 model.

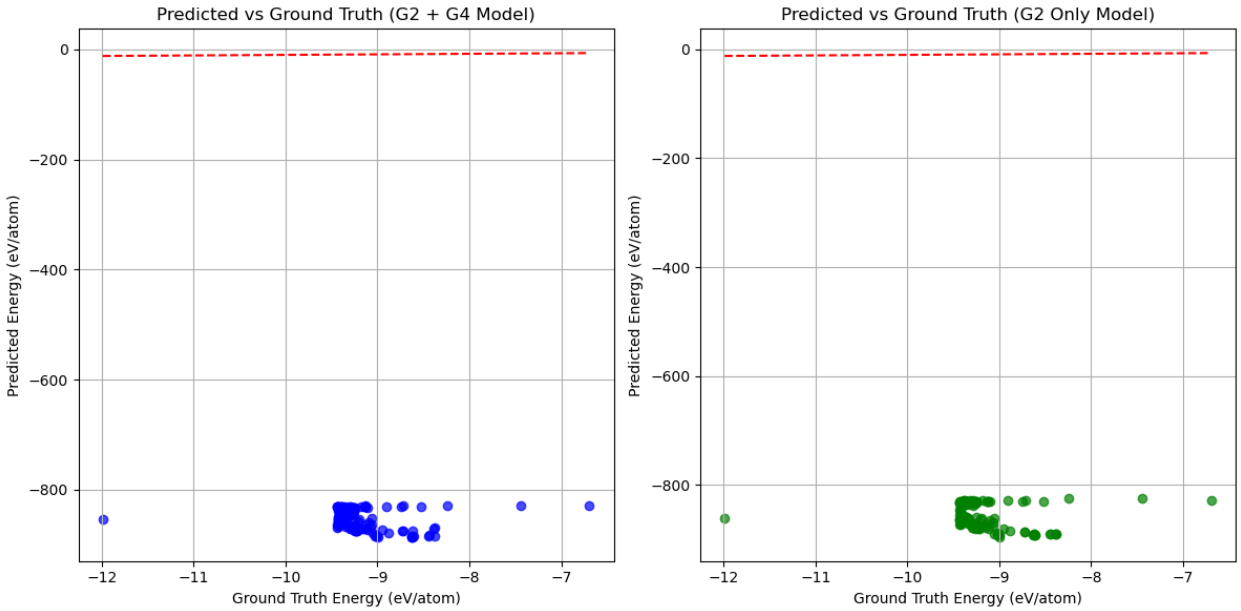

Figure 13: Initial prediction of other titanium oxides. There is a large discrepancy in the form of an offset.

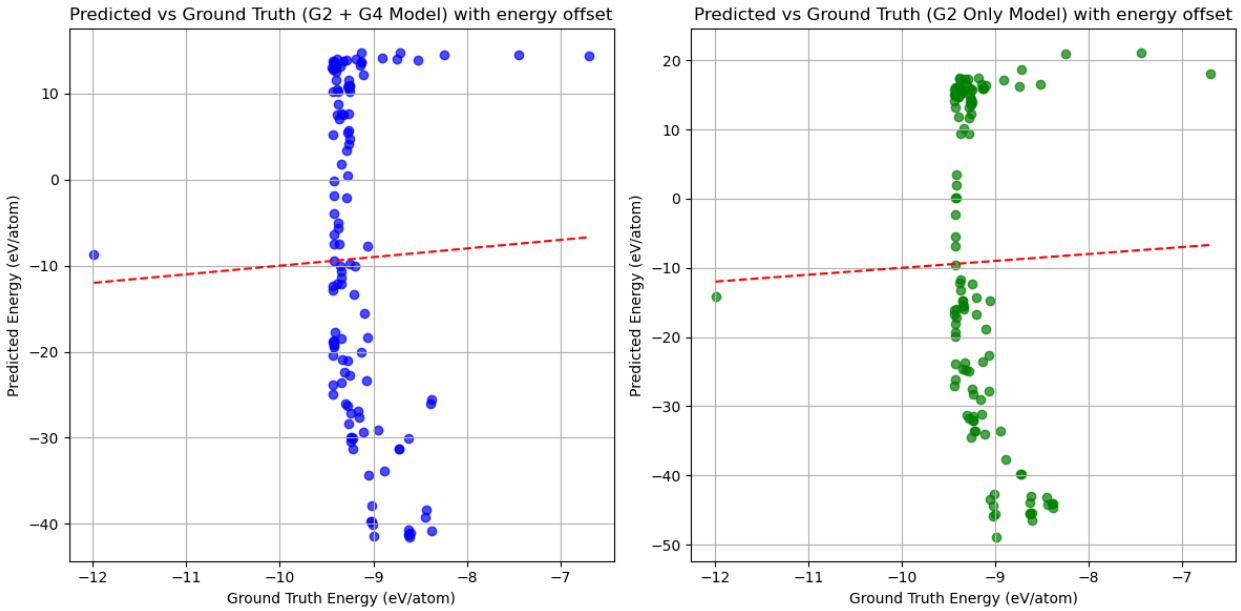

Figure 14: Predictions of other titanium oxides with an energy offset.

Metric	G^2 and G^4 Model (offset)	G^2 Only Model (offset)
MAE	16.8865	21.0413
RMSE	18.8919	23.1158

Table 5: Comparison of error metrics between G2+G4 and G2-only models after energy offset adjustment.

4 Discussion and Summary

There are two main achievements of this paper with regards to the TiO_2 models: results of Artrith and Urban were replicated within an order of magnitude, which is remarkable considering the magnitude of the energies. The G^2 symmetry function is also shown to be more relevant than the G^4 symmetry function, showing that radial interatomic distances are likely more relevant than angular measures.

However, generalizing the results of the bulk titanium dioxide to single titanium oxide crystals yielded poor results. The difficulty of this was already stated by Behler and Parinello [3] – in the seminal 2007 paper, it is remarked that the bulk silicon trained potential does not generalize well to silicon clusters. As shown, there are some trends noted in the higher energy titanium oxides, but most of them do not show any great amount of prediction by the models developed in this paper.

Further results can be developed for more similar materials to the dataset trained on in this paper, such as bulk titanium oxides that have similar structure or chemical properties (e.g. oxidation number) to the atoms in the TiO_2 sample. Furthermore, a focused study on the efficacy of different symmetry functions may yield more interesting information on the importance of each symmetry function, which may be compared to the observed structure of the species.

References

[1] Dominik Marx and Jürg Hutter. *Ab Initio Molecular Dynamics: Basic Theory and Advanced Methods*. Cambridge University Press, Apr. 2009. ISBN: 9781107663534. DOI: 10.1017/cbo9780511609633. URL: http://dx.doi.org/10.1017/CBO9780511609633.

[2] Gotthard Seifert and Kerstin Krüger. "Density Functional Theory, Calculations of Potential Energy Surfaces and Reaction Paths". In: *The Reaction Path in Chemistry:*

Current Approaches and Perspectives. Springer Netherlands, 1995, pp. 161–189. ISBN: 9789401585392. DOI: 10.1007/978-94-015-8539-2_8. URL: http://dx.doi.org/10.1007/978-94-015-8539-2_8.

[3] Jörg Behler and Michele Parrinello. "Generalized Neural-Network Representation of High-Dimensional Potential-Energy Surfaces". In: *Physical Review Letters* 98.14 (Apr. 2007). ISSN: 1079-7114. DOI: 10.1103/physrevlett.98.146401. URL: http://dx.doi.org/10.1103/PhysRevLett.98.146401.

[4] Jörg Behler. "Atom-centered symmetry functions for constructing high-dimensional neural network potentials". In: *The Journal of Chemical Physics* 134.7 (Feb. 2011). ISSN: 1089-7690. DOI: 10.1063/1.3553717. URL: http://dx.doi.org/10.1063/1.3553717.

[5] Jörg Behler. "Constructing high-dimensional neural network potentials: A tutorial review". In: *International Journal of Quantum Chemistry* 115.16 (Mar. 2015), pp. 1032–1050. ISSN: 1097-461X. DOI: 10.1002/qua.24890. URL: http://dx.doi.org/10.1002/qua.24890.

[6] Nongnuch Artrith and Alexander Urban. "An implementation of artificial neural-network potentials for atomistic materials simulations: Performance for TiO2". In: *Computational Materials Science* 114 (Mar. 2016), pp. 135–150. ISSN: 0927-0256. DOI: 10.1016/j.commatsci.2015.11.047. URL: http://dx.doi.org/10.1016/j.commatsci.2015.11.047.

[7] Kevin Ryczko et al. "Convolutional neural networks for atomistic systems". In: *Computational Materials Science* 149 (June 2018), pp. 134–142. ISSN: 0927-0256. DOI: 10.1016/j.commatsci.2018.03.005. URL: http://dx.doi.org/10.1016/j.commatsci.2018.03.005.

[8] Richard H. Duncan Lyngdoh, Henry F. Schaefer, and R. Bruce King. "Metal–Metal (MM) Bond Distances and Bond Orders in Binuclear Metal Complexes of the First Row Transition Metals Titanium Through Zinc". In: *Chemical Reviews* 118.24 (Dec. 2018), pp. 11626–11706. ISSN: 1520-6890. DOI: 10.1021/acs.chemrev.8b00297. URL: http://dx.doi.org/10.1021/acs.chemrev.8b00297.

[9] Kangkai Hu et al. “Characteristics and performance of rutile/anatase/brookite TiO2 and TiO2–Ti2O3(H2O)2(C2O4)·H2O multiphase mixed crystal for the catalytic degradation of emerging contaminants”. In: *CrystEngComm* 22.6 (2020), pp. 1086–1095. ISSN: 1466-8033. DOI: 10.1039/c9ce01694e. URL: http://dx.doi.org/10.1039/C9CE01694E.

[10] S. V. Borisov, S. A. Magarill, and N. V. Pervukhina. “Crystallographic Analysis of TiO2 Polymorphism (Brookite, Anatase, Rutile)”. In: *Journal of Structural Chemistry* 60.11 (Nov. 2019), pp. 1783–1789. ISSN: 1573-8779. DOI: 10.1134/s0022476619110118. URL: http://dx.doi.org/10.1134/S0022476619110118.

A Code Listing

All code is accessible here